Combined ac photocurrent and photothermal reflectance measurements in semiconducting *p-n* junctions. II

Andreas Mandelis, Alan A. Ward, and K. Timothy Lee
Photoacoustic and Photothermal Sciences Laboratory, Department of Mechanical Engineering and Ontario Laser and Lightwave Research Center, University of Toronto, Toronto, Ontario M5S 1A4, Canada

(Received 12 December 1988; accepted for publication 8 August 1989)

The ac photocurrent (PC) and photothermal reflectance (PTR) spectroscopic response theory of a semiconducting *p-n* junction developed in part I [J. Appl. Phys. **66**, 5572 (1989)] is applied to theoretical simulations to identify the influence of the various electronic and geometrical device parameters involved. The theory is further tested in an experimental configuration with a commercial solar cell. The experimental ac photocurrent and photothermal reflectance data exhibited satisfactory agreement with the theoretical model, and yielded, respectively, experimental values for the minority lifetimes τ_p and τ_n. A combination of PC and PTR data yielded reasonable L_n estimates.

I. INTRODUCTION

In part I of this work[1] a coupled theory was developed for measuring electronic transport parameters in *p-n* junction devices using ac photocurrent (PC) and photothermal reflectance (PTR) detection.[2] Formally, an important feature of the theory was the emergence of the PTR signal as a dependent effect, requiring complete knowledge of the carrier density fields, so as to fully describe the heat generation source term [see part I, Eqs. (69) and (70)], and also to satisfy the boundary condition involving the rate of heat generation at the surface due to nonradiative surface recombination processes.[3] The formalism for the *p-n* junction ac photocurrent generation was developed and used as the primary vehicle for providing the desirable minority-carrier distribution functions $\Delta n_p(x)$ and $\Delta p_n(x)$ on either side of the junction at $x = 0$ (see part I, Fig. 1).

In view of the above theoretical relationship between ac PC and PTR signals, the question of the possibility of complete equivalence between these two analytical methods must be addressed. In that case one of the two methods might prove redundant, although a tradeoff clearly exists between the relative theoretical simplicity of the ac PC method, and the relative experimental simplicity of the ac PTR method: the latter requires no contact electrodes for the characterization of the *p-n* junction and thus has the potential to become a promising nonintrusive characterization method at various stages of junction device fabrication.

In this work, several illustrative computer simulations of the full ac PC and PTR theories of part I will be described. The results of the comparison between the two techniques show that they *do not* yield equivalent information in a redundant manner, but, instead, each technique exhibits different degrees of sensitivity to the device electronic and geometrical parameters. Therefore, they prove to be complementary techniques in practice. Preliminary measurements using a Si solar cell will also be described from the viewpoint of electronic parameter predictions through comparisons of the ac PC and PTR experimental data with the model.

II. ac *p-n* JUNCTION PHOTOCURRENT SIMULATIONS

Measuring ac photocurrents across an illuminated *p-n* junction is a simpler operation than measuring photovoltages. The latter involve the contribution of the junction capacitance[4] at high frequencies, which tends to complicate the frequency dependence of the junction response.[5] In what follows, computer simulations of the junction generation current density J_G will be presented. Experimentally, it is the amplitude $|J_G|$ and phase Θ_G of the photocurrent signal that is monitored through lock-in detection. Therefore, the polar coordinate representation [see part I, Eqs. (29) and (30)] has been adopted throughout.

The dependence of the ac PC signal on the optical absorption coefficient β of the junction material has been investigated in Fig. 1. A Si *p-n* junction has been assumed with typical crystalline Si solar cell properties.[6] Modulation frequencies in the 0.1–10 MHz range were chosen, since they are realistic with PTR instrumentation using acousto-optic pump laser beam intensity modulation.[7,8] Figure 1 shows (in units of $qN_0/2$), a linear dependence of a PC signal on β within a range spanning the transparent end up to a maximum limit, which is an increasing function of modulation frequency f. The PC signal is seen to plateau briefly at high β and to decrease for values of $\beta \gtrsim 10^7\ \mathrm{m}^{-1}$. In that range $\beta d > 1$ and the *p*-type side of the junction (see part I, Fig. 1) becomes optically opaque, with the consequence that photogenerated minority carriers lie closer to the device surface where they are swept out of the circuit due to the high recombination velocity. Thus J_G diminishes, and Fig. 1 can be very useful in optimizing the excitation wavelength of a given *p-n* junction for maximum ac PC output through the dependence of optical absorption coefficient on λ, in the presence of high surface recombination velocities. It ought to be remarked that Fig. 1 further indicates that the ac PC technique may be used as a spectroscopic method for measuring values of $\beta(\lambda)$ lying within the linear regime ($\beta \lesssim 10^5\ \mathrm{m}^{-1}$). In Fig. 1 it was assumed that $\tau_n = 1\ \mu\mathrm{s}$. Computer simulations show that a general feature of the developed ac PC theory is its relative insensitivity to the minority electron lifetime τ_n in

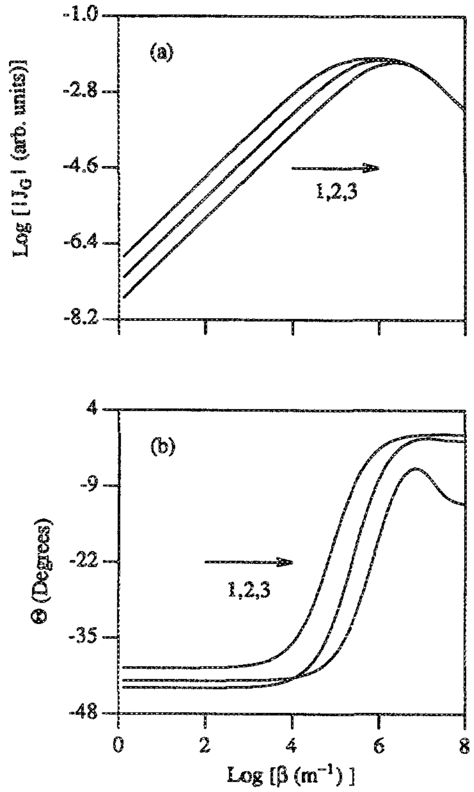

FIG. 1. ac PC dependence on substrate optical absorption coefficient β at three modulation frequencies; curve 1: 0.1 MHz; curve 2: 1 MHz; curve 3: 10 MHz. Parameters: $v_s = 10^{11}$ cm/s; $\tau_n = 1\ \mu$s; $\tau_p = 10\ \mu$s; $d = 0.2\ \mu$m; $D_n = 2$ cm^2/s; $D_p = 1$ cm^2/s. (a) Amplitude; (b) phase.

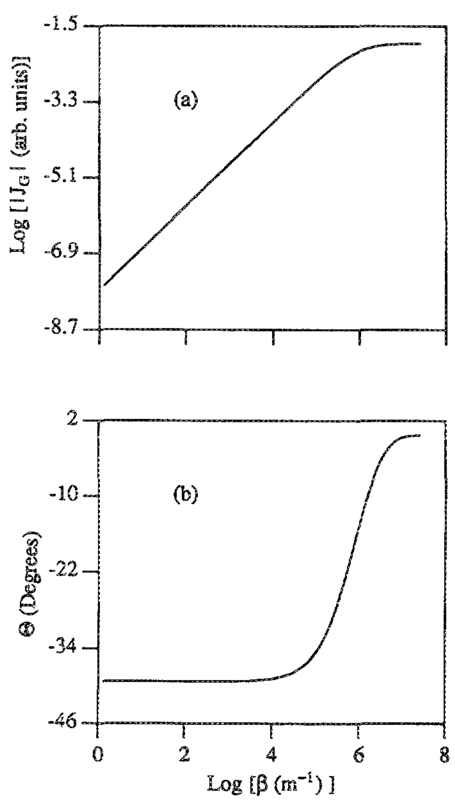

FIG. 2. ac PC dependence on substrate optical absorption coefficient β at $f = 10$ MHz. Parameters as in Fig. 1, except for $v_s = 0$ cm/s. (a) Amplitude; (b) phase.

the p layer: further manipulations of the various curves in Fig. 1 with $0.1\ \mu\text{s} \leqslant \tau_n \leqslant 0.1$ s showed little sensitivity to τ_n. Figure 2 shows the β dependence of the ac PC signal in the limit $v_s = 0$ cm/s. The high absorption-coefficient side does *not* exhibit a maximum and saturates, instead, for $\beta \gtrsim 10^5$ cm^{-1}. This is due to the fact that all the incident photons are expended in creating minority carriers, which are efficiently collected and contribute to the photocurrent as a result of zero recombination velocity.

Figure 3 shows the PC signal dependence on modulation frequency for different absorption coefficients in the high v_s limit. An inversion in amplitude of the PC response in going from the $\beta = 10^4$ cm^{-1} to the $\beta = 10^6$ cm^{-1} curve is observed, in agreement with Fig. 1. The flat response at low frequencies is characteristic of actual device behavior[5] and is a result of the fact that the modulation frequency is low compared to the recombination rate (the inverse lifetime) of the photogenerated carriers.[9,10] At high frequencies, such that $\omega\tau_p \gg 1$, i.e., $f \gg 1/2\pi\tau_p \equiv f_c = 1.59 \times 10^4$ Hz, the transparent samples ($\beta = 1$, 10^2 cm^{-1} in Fig. 3) exhibit a $f^{-1/2}$ decay, as per the discussion associated with Eq. (41), part I, upon substituting $L_{\omega p}$ for L_p. This slope has been observed experimentally by Munakata *et al.*,[5] after their data is corrected for plotting the photocurrent, rather than the photovoltage, reponse. The high-β sample response decay with f occurs at even higher frequencies, according to condition (53), part I. The extended flat nature of the high-β

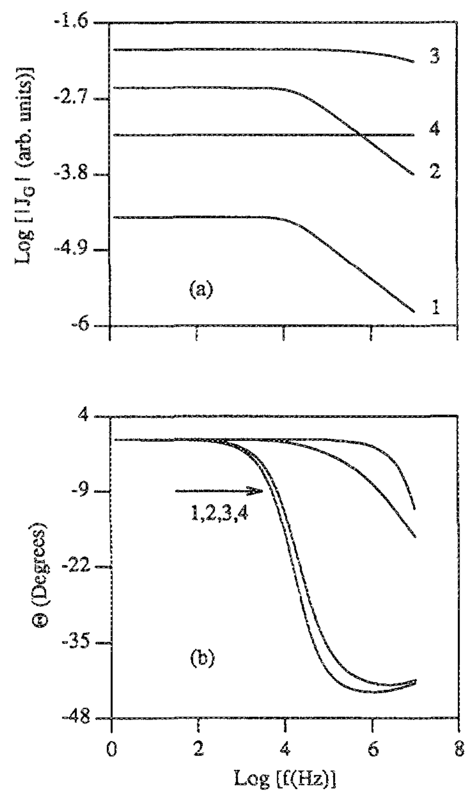

FIG. 3. ac PC frequency response at various excitation wavelengths corresponding to different optical absorption coefficients: curve 1: $\beta = 1$ cm^{-1}; curve 2: $\beta = 10^2$ cm^{-1}; curve 3: $\beta = 10^4$ cm^{-1}; curve 4: $\beta = 10^6$ cm^{-1}. Parameters: $v_s = 10^{11}$ cm/s; $\tau_n = 1\ \mu$s; $\tau_p = 10\ \mu$s; $d = 0.2\ \mu$m; $D_n = 2$ cm^2/s; $D_p = 1$ cm^2/s. (a) Amplitude; (b) phase.

frequency response is also seen in the PC phase, Fig. 3(b): physically, the response is in-phase with the excitation oscillation up to frequencies such that the minority carrier (electrons in the p side) ac diffusion length, $\mu_n(\omega)$, Eq. (46) in part I, becomes comparable to the optical absorption depth μ_β in the semiconductor. This frequency regime may be labeled *electronically thick*, in view of the analogy between the minority-carrier diffusion wave and the well-known thermal diffussion wave formalism.[11] Opsal and Rosencwaig have observed similar behavior in treating theoretically the simpler case of thermal and ambipolar electron-hole plasma diffusion waves in a uniform semiconductor substrate.[7]

Figure 4 shows the effect of the minority hole lifetime τ_p on the n side of the junction (see Fig. 1, part I) for a transparent sample. Due to the high sensitivity of the ac PC to the value of τ_p, this parameter may be calculated from experimental data by constructing a log-log plot similar to Fig. 4 and extrapolating the flat (low frequency) and straight decay (high frequency; slope $-1/2$) sections of the response until they intersect at some frequency f_c. Then, to a very good approximation, τ_p can be given by

$$\tau_p = 1/2\pi f_c. \tag{1}$$

Consistently with the simulations of Fig. 1, the shape of the p-n junction frequency response is determined by τ_p, with no apparent effect of the value of the minority electron lifetime on the p side. Upon setting $\tau_p = 10^{-5}$ s, the simulations of Fig. 4 were repeated for $10^{-5}\ \mathrm{s} \geqslant \tau_n \geqslant 10^{-8}$ s. All generated curves were identical to the relevant curve on Fig. 4. This feature is the result of the overwhelming statistical importance of the minority hole distribution on the n side due to its semi-infinite extent (see Fig. 1, part I) in comparison with the shallow thickness of the p side. Under these geometrical conditions

$$L_n = 14.1\ \mu\mathrm{m} \gg d = 0.2\ \mu\mathrm{m}, \tag{2}$$

which makes the PC signal independent of τ_n for frequencies

$$f < f_n \equiv (L_n^2 - d^2)^{1/2}/2\pi\tau_n d = 11.2\ \mathrm{MHz}. \tag{3}$$

Further simulations using the optical properties of the sample of Fig. 4 and varying the surface recombination velocity showed that the ac PC response is only slightly sensitive to that parameter and only at very high modulation frequencies; for instance, the phase shift between $v_s = 0$ and 10^{10} cm/s was only $\sim 2°$ at 10 MHz, while all amplitude and all phase curves coincided at $f \leqslant 10^5$ Hz. The inherent insensitivity of the ac PC technique to the electron transport parameters τ_n and v_s of the p-n junction irradiated in the transparent region, render this method very desirable for measuring τ_p. It is important to note that Munakata *et al.* proved the foregoing remark experimentally[5] relying on semiempirical relationships,[4] without a rigorous theoretical guarantee that the measured lifetime of minority carriers on the far side of the junction was a properly accessible quantity whose value is not affected by interference from other transport parameters of the device.

Figure 5 shows the simulation of the effects of the minority hole lifetime τ_p on a semiconducting sample in the opaque region with $\beta = 4\times 10^4\ \mathrm{cm}^{-1}$. This value was chosen so as to reflect the room temperature optical absorption coefficient of crystalline Si at the 488-nm excitation wavelength[12] of the cw Ar^+ laser used for the experiments reported in this work. The response decay at the high modulation frequency end is governed by Eq. (60), part I, i.e., a $\ln|J_G|$ vs $\sqrt{f}$ plot of the data in Fig. 5 produces an approximately

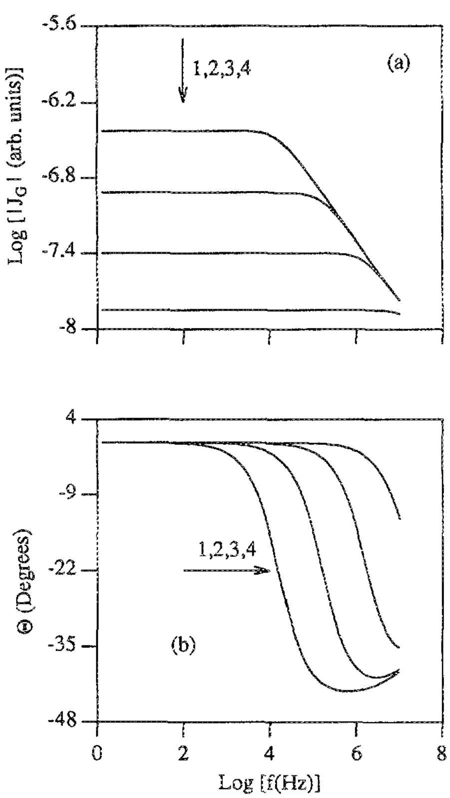

FIG. 4. ac PC frequency response of a transparent semiconductor p-n junction ($\beta = 10^{-2}\ \mathrm{cm}^{-1}$) as a function of the minority hole lifetime on the n side: curve 1: $\tau_p = 10^{-5}$ s; curve 2: $\tau_p = 10^{-6}$ s; curve 3: $\tau_p = 10^{-7}$ s; curve 4: $\tau_p = 10^{-8}$ s. Parameters: $v_s = 0$ cm/s; $\tau_n = 10^{-6}$ s; $d = 0.2\ \mu$m; $D_n = 2$ cm^2/s; $D_p = 1$ cm^2/s. (a) Amplitude; (b) phase.

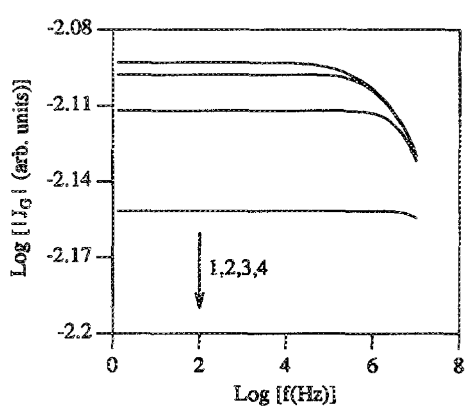

FIG. 5. PC amplitude frequency response of a Si p-n junction irradiated at 488 nm ($\beta = 4\times 10^4\ \mathrm{cm}^{-1}$) as a function of the minority hole lifetime on the n side: curve 1: $\tau_p = 10^{-5}$ s; curve 2: $\tau_p = 10^{-6}$ s; curve 3: $\tau_p = 10^{-7}$ s; curve 4: $\tau_p = 10^{-8}$ s. Parameters: $v_s = 10^{11}$ cm/s; $\tau_n = 1\ \mu$s; $d = 0.2\ \mu$m; $D_n = 2$ cm^2/s; $D_p = 1$ cm^2/s.

straight line with slope given by

$$S = -(\pi/D_n)^{1/2}d. \tag{4}$$

Figure 5 is indicative of the sensitivity of the ac PC technique to the τ_p value. Although not so straightforward a τ_p calculation as that obtained with data in the transparent region (see Fig. 4), a strong correlation exists between the value of τ_p and the turning frequency f_c of the curves in Fig. 5; an evaluation of f_c from the plot was found to yield τ_p values through Eq. (1), within a factor of 2 from the true value. A higher degree of accuracy requires fitting of Eq. (29), part I to the data.

A change in the v_s value in the opaque limit induces significant changes to the frequency response curves, however, these are essentially rigid translations along the $\log|J_G|$ axis (see Fig. 6); changing v_s from 10^{11} to 0 cm/s in Fig. 5 increases all signals by a factor of 1.5. Such an increase is expected with decreasing surface recombination velocity and is an indication of efficient current production from photogenerated minority carriers reaching the outer surface of the device. The fact that, under irradiation with highly absorbed photons, the *p-n* junction is more sensitive to the value of v_s than in the transparent case is a manifestation of the much decreased optical penetration depth, accompanied by the statistically increased importance of the surface as a recombination site. Therefore, it can be expected that v_s information may be obtained from ac PC experiments in the opaque regime and *not* from experiments in the transparent regime.

The v_s effect on the PC phase [Fig. 6(b)] is much less pronounced than the effect on amplitude. This can be understood (i) from the nature of surface recombination as a mechanism depleting the absolute number of carriers available for conduction in the external circuit, and (ii) recalling the fact that the PC amplitude is proportional to that number, whereas the PC phase is a ratio of two amplitudelike quantities (in-phase and quadrature components). As such, the strong dependence on number of carriers essentially cancels out from numerator and denominator of the phase channels [see Eq. (30), part I].

The effect of τ_n enters the PC generation mechanism *via* the relationship between L_n and d, as shown in inequalities (2) and (3). Since those relations are not dependent on the value of β, no change is expected in the degree of signal insensitivity to τ_n under illumination corresponding to high values of β. This expectation was borne out with simulations of curves in Fig. 5 using 10^{-8} s $\leqslant \tau_n \leqslant 0.1$ s.

An interesting combination of the effects of varying the junction depth d and the surface recombination velocity on the PC amplitude is further shown in Fig. 7. Under high surface recombination conditions, Fig. 7(a), increasing the

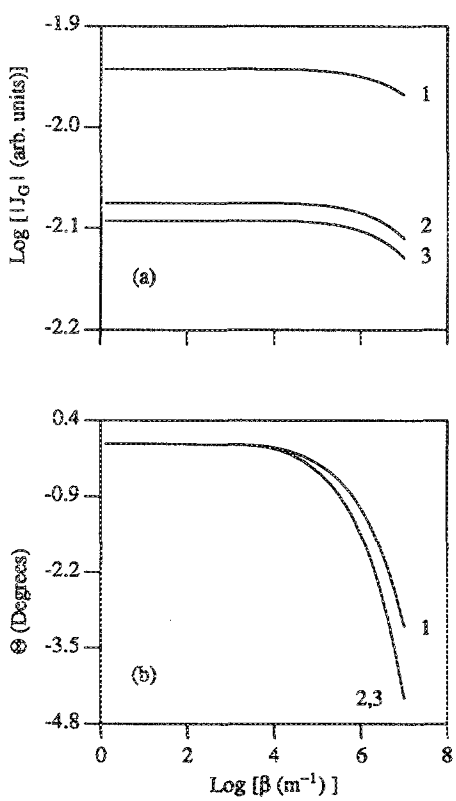

FIG. 6. ac PC frequency-response dependence on v_s under optical excitation with strongly absorbed photons in Si ($\beta = 4\times 10^4$ cm^{-1}): curve 1: $v_s = 10^4$ cm/s; curve 2: $v_s = 10^6$ cm/s; curve 3: $v_s = 10^8$ cm/s; and $v_s = 10^{10}$ cm/s. Parameters: $\tau_p = 10^{-5}$ s; $\tau_n = 1$ μs; $d = 0.2$ μm; $D_n = 2$ cm^2/s; $D_p = 1$ cm^2/s. (a) Amplitude; (b) phase.

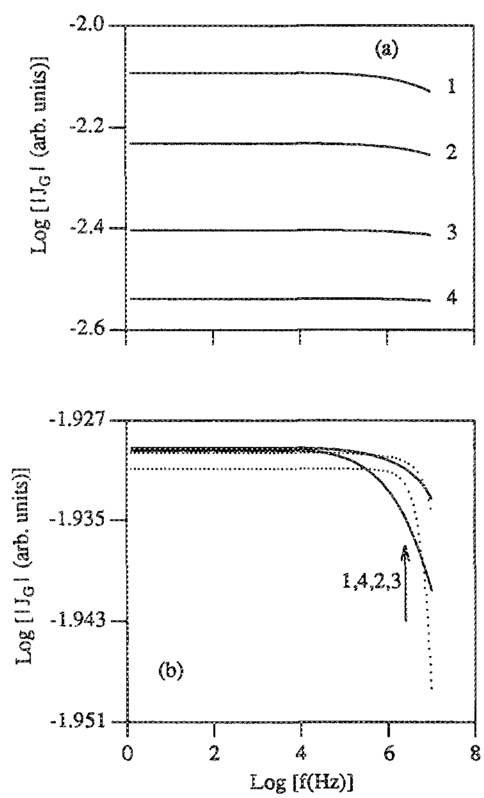

FIG. 7. PC amplitude frequency response of a Si *p-n* junction irradiated as in Fig. 5. (a) $v_s = 10^{11}$ cm/s; curve 1: $d = 0.2$ μm; curve 2: $d = 0.4$ μm; curve 3: $d = 0.7$ μm; curve 4: $d = 1$ μm; (b) $v_s = 0$ cm/s; curve 1: $d = 0.4$ μm; curve 2: $d = 0.7$ μm; curve 3: $d = 1$ μm; curve 4: $d = 1.5$ μm. Parameters: $\beta = 4\times 10^4$cm^{-1}; $\tau_p = 10^{-5}$ s; $\tau_n = 1$ μs; $D_n = 2$ cm^2/s; $D_p = 1$ cm^2/s.

junction depth decreases substantially the PC. A larger fraction of the photocarriers is surface depleted as d becomes comparable to the minority electron diffusion length L_n, and relation (2) no longer holds. With increasing values of d, the effects of τ_p on the far side of the junction become less important in determining the shape of the frequency response curve, since optical penetration to the junction depth is inhibited. As a result, the downward curvature observed in Fig. 7(a) $d = 0.2\,\mu$m curve, is gradually eliminated from the plotted frequency range when $d \cong 1\,\mu$m. Under zero surface recombination conditions, Fig. 7(b), increasing the junction depth has only a small effect on the PC amplitude, since all the photogenerated minority carriers that diffuse to the outer surface get collected efficiently there. The τ_p effect in Fig. 7(b) becomes less important with increasing d, which decreases the downward curvature of the $d = 0.7\,\mu$m curve compared to that of the $d = 0.4\,\mu$m curve. Further increase in d renders τ_n a limiting parameter as the f_n in inequality (3) decreases. The result is the emergence of new downward trends for the $d = 1$ and $1.5\,\mu$m curves, with substantial decay of the latter at $f \simeq 10$ MHz. For these curves f_n ($d = 1\,\mu$m) $= 2.2$ MHz and f_n ($d = 1.5\,\mu$m) $= 1.5$ MHz, clearly accessible within the 1–10-MHz modulation frequency range of Fig. 7(b) in which relation (3) does not hold. Under similar conditions, the effects of varying τ_n are not evident in Fig. 7(a), because the PC signal level decrease due to surface recombination overwhelms the relatively small decrease resulting from the invalidation of condition (3) in the $d = 1\,\mu$m curve.

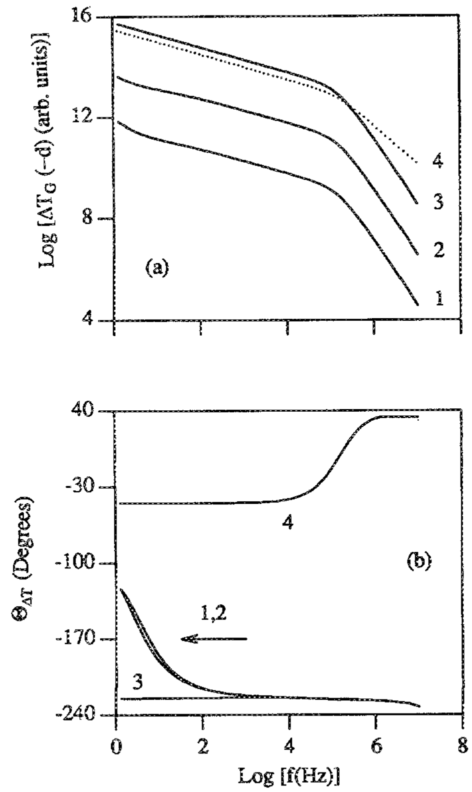

FIG. 8. PTR frequency response at various excitation wavelengths corresponding to different optical absorption coefficients: curve 1: $\beta = 10^{-2}$ cm^{-1}; curve 2: $\beta = 1$ cm^{-1}; curve 3: $\beta = 10^2$ cm^{-1}; curve 4: $\beta = 10^4$ cm^{-1}. Parameters: $v_s = 10^{11}$ cm/s; $\tau_n = 1\,\mu$s; $\tau_p = 10\,\mu$s; $d = 0.2\,\mu$m; $D_n = 2$ cm^2/s; $D_p = 1$ cm^2/s; $\alpha = 1$ cm^2/s. (a) Amplitude; (b) phase.

III. ac *p-n* JUNCTION PHOTOTHERMAL REFLECTANCE SIMULATIONS

Unlike the ac PC technique, the ac PTR response is characterized by the thermal diffusion length $\mu_t(\omega)$, in addition to all the characteristic lengths of the former method. As a result, when Eqs. (B6)–(B9), in Appendix B, part I, are plotted as a function of modulation frequency, a PTR amplitude decrease, characteristic of the one-dimensional (1D) nature of the problem, is oberved immediately upon departure from the dc level. This situation is illustrated for various values of the optical absorption coefficient in Fig. 8, which is to be compared with the PC signals of Fig. 3. The thermal diffusivity value for crystalline Si was used in Fig. 8 and all subsequent numerical simulations. The low-frequency range is thermal diffusion length-dominated and the PTR signal decreases as $f^{-1/2}$, as predicted by Eq. (88), part I, for the optically opaque limit. Figure 8 indicates that PTR curves corresponding to all the considered spectral values exhibit essentially the same frequency behavior at low f. The steeper decay of the low-β curves observed at very low frequencies with an apparent "break" at ~ 10 Hz is due to the fact that, with increasing f, the thermal contribution to the PTR signal decreases rapidly, whereas the density of photogenerated carriers remains unchanged. Thus, the PTR signal is dominated by the photocarrier contribution at $f > 10$ Hz. The low-β phase curves in Fig. 8(b) also exhibit the thermal-to-electronic transition, with the thermal effects persisting up to ~ 1 kHz. The high-β curves do not show the low-frequency "break," as in this case the efficient optical absorption results in high density of photogenerated carriers, which dominates over any purely thermal effects. As a consequence, the high-β PTR frequency response assumes the intermediate frequency slope immediately upon departure from the dc level. Kino *et al.*[10] have observed similar tradeoffs between thermal and electronic contributions in the frequency response of photoacoustic signals from semiconductors generated using a thermal acoustic apparatus. For the $\beta = 10^4$ cm^{-1} curve the low-frequency phase saturation occurs at $-\pi/4$, Fig. 8(b), as predicted in Eq. (88), part I. The amplitude trend reversal of the PTR signal for $\beta = 10^4$ cm^{-1} (and higher β's), is due to the high v_s assumed for this simulation and may be explained using the same argument as that for the reversals observed in Figs. 1 and 3. A very important difference between Figs. 3 and 8 lies with the position (on the frequency axis) of the "knee" separating the intermediate- and high-frequency regions. The PTR plot exhibits the "knee" at a frequency $f \cong 0.1$ MHz, i.e., one order of magnitude higher than similar curves in Fig. 3. The reason for this difference is the *reversal of the roles* of τ_n and τ_p in contributing sensitively to the probing method: PTR detection being a front surface thermal technique, which weighs the minority nonradiative recombination-induced signals in an exponentially damped profile from the front surface, it is much more sensitive to near-the-surface recombination rates, governed by τ_n, than those at the far side of the junction, governed by τ_p. Therefore, the "knee" in Fig. 8 occurs at a frequency such that

$$f_c \approx 1/2\pi\tau_n = 1.59 \times 10^5 \text{ Hz}.$$

This is one order of magnitude higher than the respective "knee" in Fig. 3, reflecting the difference in the assumed values for τ_n and τ_p. To further substantiate this crucial reversal of roles of minority lifetimes between the two techniques under consideration, Fig. 9 shows the PTR frequency response of a transparent Si *p-n* junction with τ_n as a parameter. The "knees" correspond to the condition $2\pi f_c \tau_n \approx 1$, and the signal amplitude decreases with decreasing τ_n, as expected from an electron density dominated mechanism. At $\tau_n = 1\ \mu$s, the free photogenerated minority electron density is so low, that the purely thermal contribution dominates at low frequencies and the "break" at ~ 10 Hz reappears, as discussed in the context of Fig. 8. The signal phase of the $\tau_n = 1\ \mu$s curve, Fig. 9(b), also departs substantially from the electronic contribution dominated baseline owing to purely thermal-wave effects.

Figure 10 shows the effects of varying τ_p on the transparent region PTR signal. As the incident radiation penetrates deep into the body of the device, much deeper than the junction depth d, the actual value of τ_p does have some effect of the PTR signal at low frequencies; it is only in this frequency range that thermal communication to the surface from the bulk may be effected, since $\mu_t(\omega)$ is larger than, or

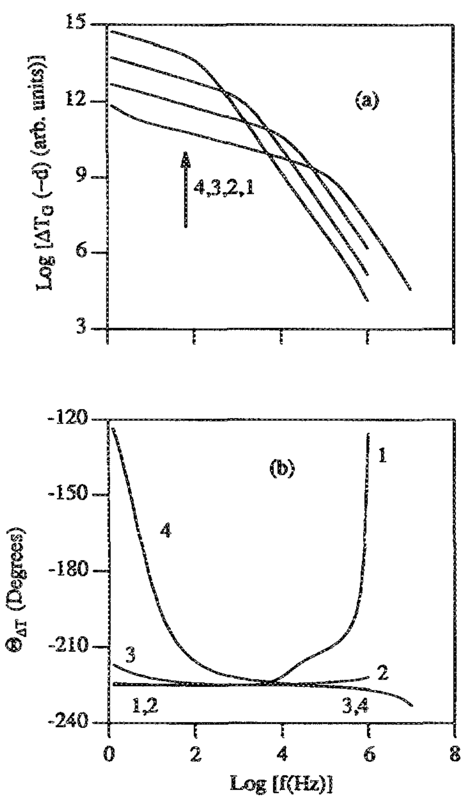

FIG. 9. PTR frequency response of a transparent Si *p-n* junction ($\beta = 10^{-2}$ cm^{-1}) as a function of the minority electron lifetime on the *p* side: curve 1: $\tau_n = 10^{-3}$ s; curve 2: $\tau_n = 10^{-4}$ s; curve 3: $\tau_n = 10^{-5}$ s; curve 4: $\tau_n = 10^{-6}$ s. Parameters: $v_s = 10^{11}$ cm/s; $\tau_p = 10^{-5}$ s; $d = 0.2\ \mu$m; $\alpha = 1$ cm^2/s; $D_n = 2$ cm^2/s; $D_p = 1$ cm^2/s. (a) Amplitude; (b) phase.

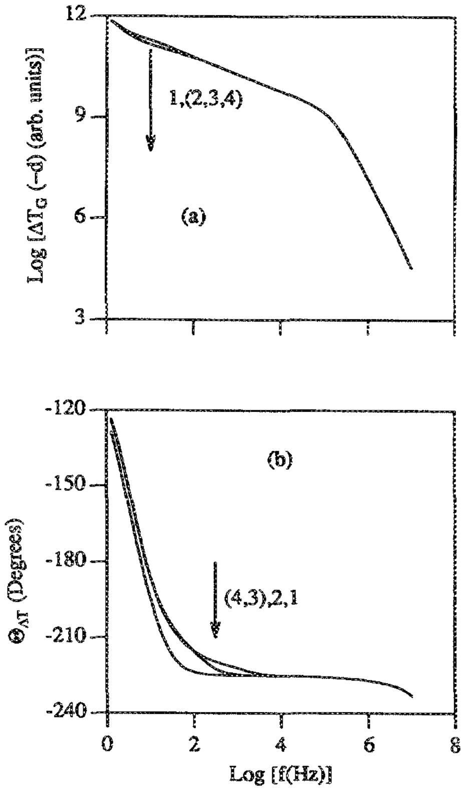

FIG. 10. PTR frequency response at a transparent Si sample of Fig. 9 as a function of the minority hole lifetime on the *n* side: curve 1: $\tau_p = 10^{-2}$ s; curve 2: $\tau_p = 10^{-3}$ s; curve 3: $\tau_p = 10^{-4}$ s; curve 4: $\tau_p = 10^{-5}$ s. $\tau_n = 1\ \mu$s for all curves. (a) Amplitude; (b) phase.

comparable to, d and $\mu_p(\omega)$. The high-frequency "knee" is solely determined by the τ_n value, and the PTR amplitude for all curves with $\tau_p \lesssim 10^{-3}$ s is practically identical. The phase exhibits somewhat better τ_p resolution than the amplitude, however, it becomes degenerate for all values of $\tau_p < 10^{-4}$ s.

Figure 11 is the high-β counterpart of Fig. 9. In this case, the condition $L_n \gg \mu_\beta$ holds for all curves. As a result, the electronic contribution to the photothermal signal is the same, as long as $\mu_t(\omega) \gg d$, and all curves follow the $f^{-1/2}$ dependence, as predicted by Eq. (88), part I. At frequencies such that $\omega_c \tau_n \approx 1$ the slope increases to approximately $f^{-3/2}$ dependence and "knees" appear from which the value of τ_n may be calculated from experimental curves. The phase data also exhibit appropriate shifts from the $-\pi/4$ baseline [Eq. (88), part I] [see Fig. 11(b)], corresponding to recombination delay times. At very high frequencies, such that $\omega_c \tau_n \gg 1$, Eqs. (96) and (97), part I, indicate that the PTR signal levels become independent of τ_n due to the term proportional to L_n^2/τ_n. Therefore, all amplitude curves converge to the same line *at a different level* from the low-frequency limit [see Fig. 11(a)], whereas all phase curves tend to return to the low-frequency baseline at $-\pi/4$. Physically, at $f \gg f_c$ there is little thermal energy released to the solid as a result of carrier recombination and thus the PTR signal is solely due to direct lattice heating, with a fraction of the optical energy stored at the excited free electronic gas. For the same substrate material, all different τ_n curves converge

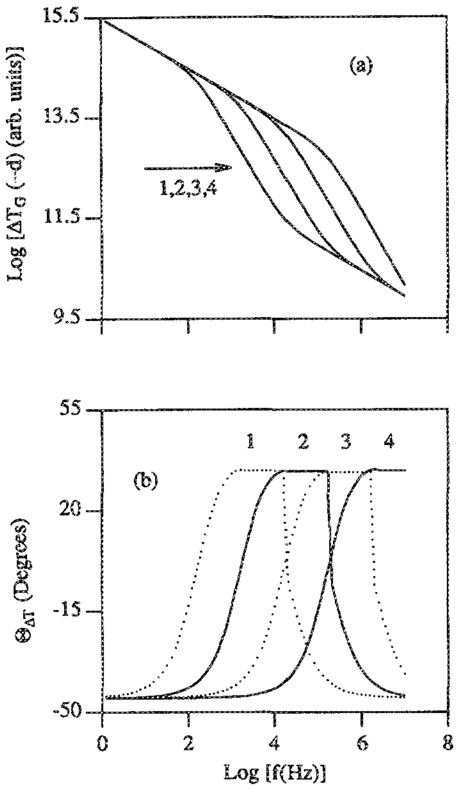

FIG. 11. PTR frequency response at an opaque Si p-n junction ($\beta = 10^4$ cm^{-1}) as a function of the minority electron lifetime on the p side: curve 1: $\tau_n = 10^{-3}$ s; curve 2: $\tau_n = 10^{-4}$ s; curve 3: $\tau_n = 10^{-5}$ s; curve 4: $\tau_n = 10^{-6}$ s. Parameters: $v_s = 10^{11}$ cm/s; $\tau_p = 10^{-5}$ s; $d = 0.2$ μm; $\alpha = 1$ cm^2/s; $D_n = 2$ cm^2/s; $D_p = 1$ cm^2/s. (a) Amplitude; (b) phase.

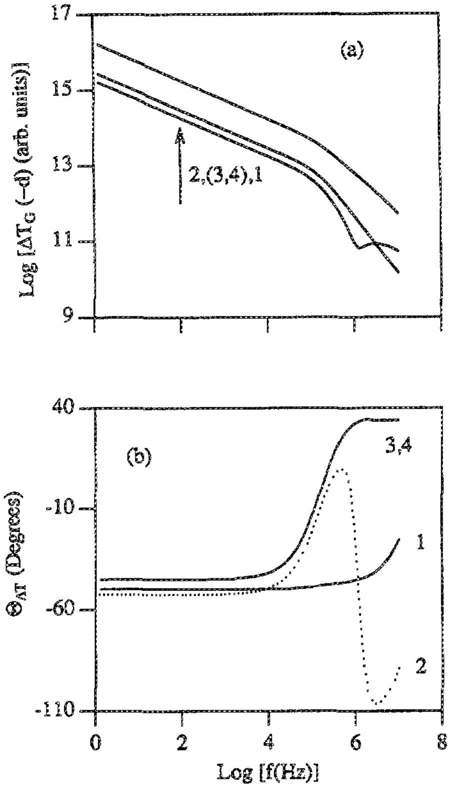

FIG. 12. PTR frequency response dependence on v_s under optically opaque conditions in Si ($\beta = 1 \times 10^4$ cm^{-1}): curve 1: $v_s = 10^2$ cm/s; curve 2: $v_s = 10^5$ cm/s; curve 3: $v_s = 10^8$ cm/s; curve 4: $v_s = 10^{11}$ cm/s. Parameters: $\tau_p = 10^{-5}$ s; $\tau_n = 1$ μs; $d = 0.2$ μm; $\alpha = 1$ cm^2/s; $D_n = 2$ cm^2/s; $D_p = 1$ cm^2/s. (a) Amplitude; (b) phase.

to the same heating level, with the same fraction of the total energy stored in the electronic system, whose photoexcited carrier density remains constant at constant β.

In the opaque limit, little light can effectively penetrate beyond the junction depth, which renders the density of photoexcited minority holes on the n side quite low, and the contribution to the PTR signal from their recombination insignificant. As a result, complete insensitivity of the PTR signal, amplitude and phase, to the actual value of τ_p over several orders of magnitude ($1\ \mu$s $\leqslant \tau_p \leqslant 0.1$ s) has been observed numerically for the curves of Fig. 11.

The PTR signal dependence on the surface recombination velocity is shown in Fig. 12 (opaque limit) and may be understood in the light of the PC simulations for a similar sample presented in Fig. 6. As v_s increases, the available photoexcited electronic density decreases substantially, as shown in Fig. 6. As a further consequence, the PTR signal, which is mainly due to nonradiative minority electron recombination on the p side, also decreases accordingly. Greater increases in v_s produce further decreases in the PC signal, however, a greater fraction of the incident energy appears synchronously at the surface as heat due to the enhanced nonradiative surface recombination. This thermal increase tends to counterbalance the signal loss due to lower free photoexcited densities. Under strong surface recombination conditions, the thermal increase due to this mechanism predominates and a PTR signal level reversal is observed ($v_s = 10^8$–10^{11} cm/s, and partially the $v_s = 10^5$-cm/s curve). These signals become independent of v_s at $v_s \geqslant 10^8$ cm/s, as all surface carriers recombine efficiently nonradiatively. At the same time the complementary fraction of photogenerated carriers that contributes to the external current remains constant, leading to PC signals independent of v_s as shown in Fig. 6, 10^8–10^{11} cm/s curves. The PTR response corresponding to $v_s = 10^5$ cm/s, Fig. 12, shows the effects of the surface thermal increase/free photocarrier density decrease tradeoff: at low frequencies the device bulk contributes substantially to the PTR signal, which is thus dominated by the photoexcited density of minority carriers recombining in the bulk. At high frequencies, the surface heating due to carriers recombining at the surface dominates and the PTR signal exhibits an enhancement with respect to the bulk-contributed value. The PTR phase, Fig. 12(b), also shows a tendency to follow the bulk-controlled, low-v_s curves at low frequencies, however, it follows the surface-controlled, high-v_s curves at $f \gtrsim 10^4$ Hz. It is important to notice that the deviation from the low-frequency, straight-line behavior of the PTR amplitudes of Fig. 12(a) occurs at the same f_c that is controlled by τ_n, Eq. (4). Therefore, τ_n information may be accurately extracted from data plots such as that of Fig. 12(a) irrespective of the state of the device surface and the actual value of v_s.

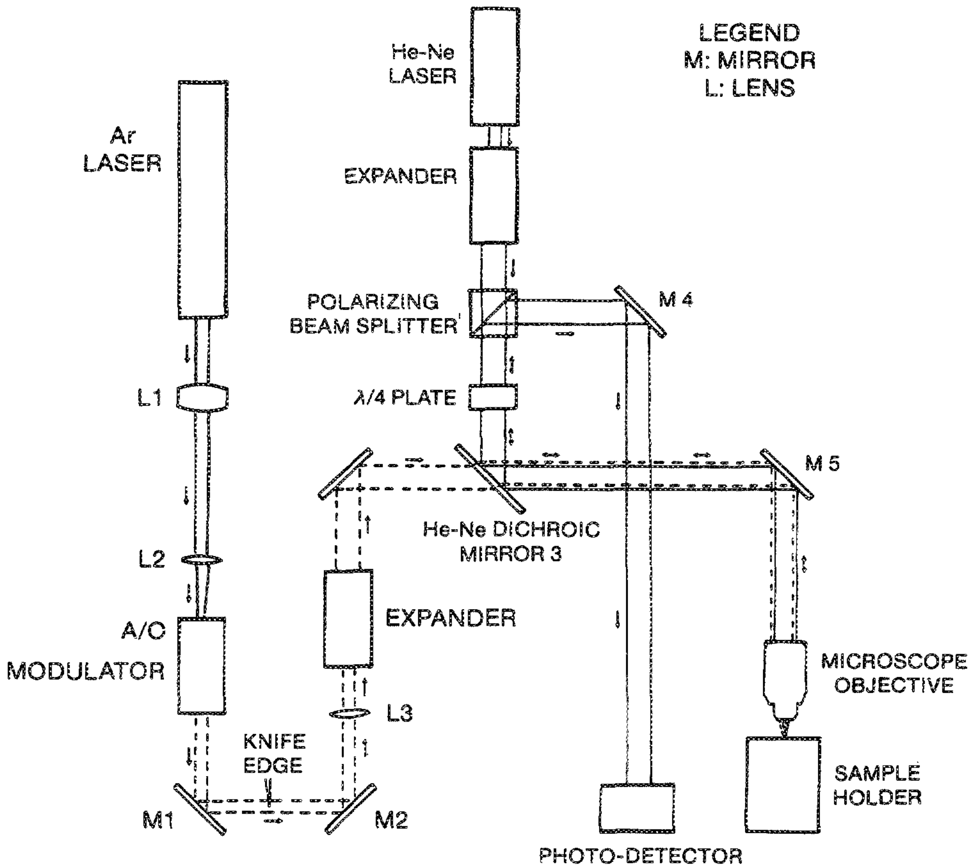

FIG. 13. Schematic diagram of PTR and PC instrumentation. The entire assembly rests on an antivibrational optical table.

IV. EXPERIMENT AND DISCUSSION

The experimental apparatus used in our preliminary experiments has been described elsewhere[8] and was similar to the instrument utilized by Opsal *et al.*[13] An outline is shown in Fig. 13. The 488-nm beam from the pump Ar^+ laser with a 20-mW output power was focused to $\sim 6\,\mu$m on the sample surface. A probe 4-mW He-Ne laser was used (632.8 nm) for the PTR measurements. The two laser beams were focused collinearly on the sample to provide a maximum thermoreflectance signal, as measured by a lock-in analyzer. All output signals were normalized by the frequency response of the combined detection electronics, which included the lock-in analyzer and the bicell photodetector.

A Si p^+/n solar cell, 150 μm thick, manufactured by Arco Solar was used as a sample. The junction depth d was nominally 0.1 μm, and an antireflection coating had been applied on the surface by the manufacturer. Ohmic leads were soldered onto the front and back of the cell for ac PC measurements. The leads were then connected across a 100-Ω resistor and the photocurrent was proportional to the voltage drop across the resistor following illumination of the cell. The ac voltage lead was connected to a lock-in amplifier input, while a second lock-in was used for simultaneous PTR measurements.

The solar cell was illuminated at 488 nm, so that β (488 nm) $\cong 4\times 10^4\ \mathrm{cm}^{-1}$ at room temperature.[12] This value of β was used for all data analysis. At high frequencies, the ac PC signal should behave according to Eq. (54), part I:

$$|J_G(f)| = C_1[\exp(-S\sqrt{f})/f], \tag{5}$$

for $v_s \to 0$. In Eq. (5) C_1 is a frequency-independent constant and S is the high-frequency slope given by Eq. (4). On the other hand, high v_s values are expected to yield a high-frequency signal according to Eq. (60), part I:

$$|J_G(f)| = C_2[\exp(-S\sqrt{f})/\sqrt{f}], \tag{6}$$

for $v_s \to \infty$. Equations (5) and (6) show that the goodness of fit of the experimental data in the form $\ln[f|J_G|(f)|]$ or $\ln[\sqrt{f}|J_G(f)|]$ vs $\sqrt{f}$ is a strong indicator of the range of values v_s appropriate for the device under consideration. Both cases were tried with the high-frequency PC amplitude response of our solar cell and a much better fit was obtained with Eq. (6) than with Eq. (5). The results are shown in Fig.

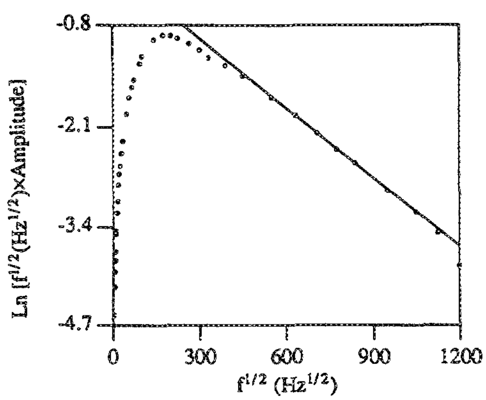

FIG. 14. High-frequency data fit to Eq. (6). High-frequency slope $S = -1.772\times 10^{-4}\ \mathrm{s}^{1/2}$.

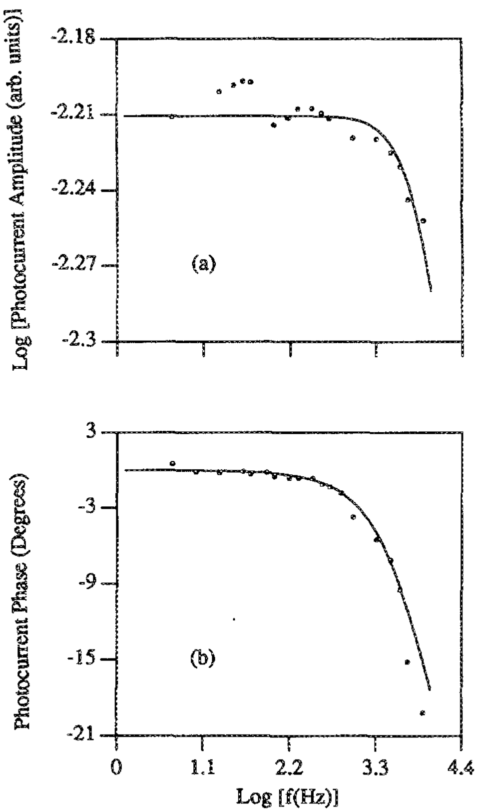

FIG. 15. Experimental data (dots) and theoretical PC frequency response of a Si solar cell. (a) Amplitude; (b) phase. Optimum $\tau_p = 30\,\mu$s.

14. The high-frequency slope S gave the minority electron diffusion coefficient value $D_n = 1 \times 10^{-2}$ cm^2/s. This low value is consistent with high surface recombination velocities[14] (possibly from high surface and near-surface defect densities), and was also used for D_p in the generation of the theoretical device frequency response. Figure 15 shows ac PC amplitude and phase data from the solar cell, as well as theoretical fits to the data using Eqs. (29) and (30), part I, with the arbitrary value $v_s = 1 \times 10^{11}$ cm/s to approximate the $v_s \to \infty$ condition suggested by the fit of Fig. 14. The agreement between experimental data and the theoretical fits for both amplitude and phase in Fig. 15 was found to be optimal using $\tau_p = 30\,\mu$s. This value is within a factor of 2 from the 40-μs rough value determined directly from extrapolations of the low- and high-frequency segments until they intersect, as discussed in conjunction with Fig. 4 earlier. This empirical procedure is approximately valid under 488-nm irradiation, since $\beta d = 0.4$, i.e., the solar cell optically lies intermediately between the transparent and opaque regions to a depth equal to d. The estimated τ_p value is in good agreement with typical values for Si solar cells.[6] The same value was used as τ_n in the fit of Fig. 15 as a preliminary estimate; it should be recalled that the PC signal was found to be insensitive to the actual τ_n value for the configuration of Fig. 1, part I. This value was updated following the analysis of the PTR data.

PTR measurements on the Si solar cell at a constant Ar^+ laser beam irradiance modulation frequency exhibited a slow decay of the amplitude over time: within a 20-min time span, the original signal amplitude tended to decay by $\sim 50\%$; the phase was somewhat less sensitive to temporal shifts. Many attempts were made to stabilize the signal, including long waiting periods for attainment of steady state. Unfortunately, it was observed that the rate of decay would diminish as a function of time, however, the signal never reached a steady state. Rosencwaig,[2] and Opsal and Rosencwaig[14] discussed similar phenomena observed in PTR experiments with Si substrate wafers. These investigators attributed the temporal dependence of the signal to diffusive removal of trapped carriers from surface defect states upon illumination,[15] a form of electronic laser annealing effect on the $\Delta R / R_0$ signal.[16] The high v_s value suggested by the ac PC portion of the present experiments is also consistent with a substantial density of carriers interacting with surface electronic defects. Rosencwaig *et al.*[16] observed temporal dependence of the signal phase as well. In the present experiments, it is likely that wafer processing for solar cell fabrication may have caused surface damage that was not entirely annealed upon completion of the manufacturing cycle. The observed diminishing signal decay rate as a function of exposure to the pump beam is certainly indicative of irreversible repair process(es) in which defect associated nonradiative contributions decrease in time. No macroscopic material damage by the 20-mW laser beam could be identified under magnification, which supported the viewpoint that optical interactions at the electronic level were occurring. The temporal behavior was essentially reproducible at different (up to 20) spots on the solar cell.

In view of the above observations, no attempt was made to fit the PTR signal with theoretical frequency response curves, however, a definite monotonic decrease with increasing frequency $\propto f^{-0.4 \pm 0.1}$ was noticed, in semiquantitative agreement with the PTR theory of part I. Figure 16 shows the experimental PTR amplitude frequency response in the 10 kHz–1 MHz range. The data were taken after long exposure of the cell to the exciting laser beam, so that the slow temporal decay was minimal throughout the experiment. Low-frequency data was uninteresting and undesirable from

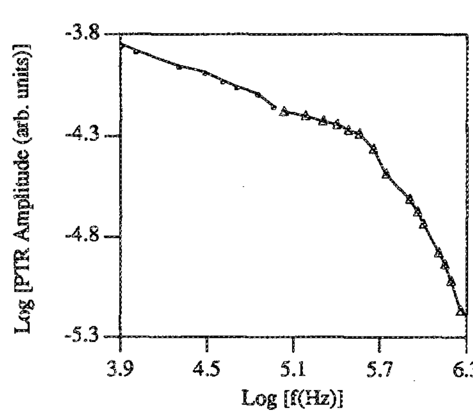

FIG. 16. Experimental PTR amplitude data of Si solar cell. Measured $\tau_n \approx 0.73\,\mu$s; closed circles signify data obtained with a low-frequency bandwidth EG&G 5204 lock-in; open triangles are data obtained with a high-frquency bandwidth EG&G 5202 lock-in.

the point of view of this experiment, as they did not yield useful parameter information. Furthermore, the accuracy of the entire frequency response curve would suffer considerably if low f data were included, as the data acquisition time became comparable, or large, compared to the slow signal decay time. The combination of a low-frequency (EG&G 5204) and a high-frequency (EG&G 5202) lock-in analyzer was required to record the data of Fig. 16. In the theoretical context of Fig. 11, the "knee" in the frequency response of Fig. 16 occurs at $f_c \cong 2.2 \times 10^5$ Hz. This corresponds to a minority lifetime $\tau_n = 0.73\ \mu s$, in good agreement with typical lifetime values in the diffused thin p^+ layer of commerical Si solar cells. This calculation, along with the PC-derived D_n value, gave $L_n = 0.85\ \mu m$, a reasonable value[6] for the diffused layer. The -0.4 ± 0.1 slope of the below the "knee" regime is strongly indicative of photothermal wave behavior, in agreement with the "ideal" -0.5 slope of Figs. 9 and 11.

V. CONCLUSIONS

In this work the salient features and diagnostic capabilities of the combination of ac PC and PTR techniques with respect to *p-n* junction device characteristics have been studied in the light of a coupled model developed in part I. An important task of the study was to ascertain the uniqueness and complementarity of each ac technique. It was found through computer simulations that the PC signal is sensitive to the bulk minority-carrier lifetime (τ_p), whereas the PTR signal is sensitive to the diffused (or implanted) thin surface layer minority-carrier lifetime (τ_n). Furthermore, the PC method proved capable of measuring the D_n value from the high-frequency slope, and of providing a strong indication as to the possible range of surface recombination velocity values. The PTR signal, especially the phase, showed improved sensitivity to the actual value of v_s and may potentially be used to measure this parameter. The combination of both techniques was thus able to give the L_n value from the measurements of D_n and τ_n values in a preliminary experimental configuration using a commercial p^+/n solar cell. The τ_p and τ_n values obtained from PC and PTR frequency response "knees" were found to be in good agreement with literature values for these parameters.

ACKNOWLEDGMENTS

The authors are grateful to the National Science and Engineering Research Council of Canada (NSERC) and to the Ontario Laser and Lightwave Research Center (OLLRC) for mutually provided partial support for this project. Thanks are also due to Robert Wagner and Kamyar Ghandi for artistic support with the figures in parts I and II.

[1]A. Mandelis, J. Appl. Phys. **66**, 5572 (1989).
[2]A. Rosencwaig, in *Photoacoustic and Thermal Wave Phenomena in Semiconductors*, edited by A. Mandelis (North-Holland, New York, 1987), Chap. 5.
[3]J. R. Meyer, F. J. Bartoli, and M. R. Kruer, Phys. Rev. B **21**, 1559 (1980).
[4]C. Munakata, K. Yagi, T. Warabisako, M. Nanba, and S. Matsubara, Jpn. J. Appl. Phys. **21**, 624 (1982).
[5]C. Munakata, N. Honma, and H. Itoh, Jpn. J. Appl. Phys. **22**, L103 (1983).
[6]A. L. Fahrenbruch and R. H. Bube, *Fundamentals of Solar Cells* (Academic, New York, 1983), Chap. 7.4.
[7]J. Opsal and A. Rosencwaig, Appl. Phys. Lett. **47**, 498 (1985).
[8]A. Mandelis, A. Williams, and E. K. M. Siu, J. Appl. Phys. **63**, 92 (1988).
[9]R. G. Stearns and G. S. Kino, in *Photoacoustic and Thermal Wave Phenomena in Semiconductors*, edited by A. Mandelis (North-Holland, New York, 1987), Chap. 9.
[10]G. S. Kino, R. G. Stearns, and B. T. Khuri-Yakub, U.S. Patent No. 4,683,750 (1987).
[11]A. Rosencwaig and A. Gersho, J. Appl. Phys. **47**, 64 (1975).
[12]W. C. Dash and R. Newman, Phys. Rev. **99**, 1151 (1955).
[13]J. Opsal, A. Rosencwaig, and D. L. Williams, Appl. Opt. **22**, 3169 (1983).
[14]J. Opsal and A. Rosencwaig, in *Review of Progress in Quantitative Nondestructive Evaluation*, edited by D. O. Thompson and D. E. Chimenti (Plenum, New York, 1988), Vol. 7A, p. 215.
[15]J. Opsal, M. W. Taylor, W. L. Smith, and A. Rosencwaig, J. Appl. Phys. **61**, 240 (1987).
[16]A. Rosencwaig, J. Opsal, and M. W. Taylor, in *Review of Progress in Quantitative Nondestructive Evaluation*, edited by D. O. Thompson and D. E. Chimenti (Plenum, New York, 1987), Vol. 6A, p. 237.